Effect of Electron-Phonon Interaction on Optical Properties in One-Dimensional Mott Insulators

Takami TOHYAMA[1,*] and Hiroaki MATSUEDA[2,**]

[1] *Yukawa Institute for Theoretical Physics, Kyoto University, Kyoto 606-8502, Japan*
[2] *Sendai National College of Technology, Sendai 989-3128, Japan*

Interplay of strong electron correlation and electron-phonon interaction is one of important issues in the physics of low dimensional correlated electron systems. In order to understand the interplay, we examine the optical properties of the one-dimensional (1D) Hubbard-Holstein model at half-filling, by employing the dynamical density matrix renormalization group (DMRG) technique. We discuss the effect of the electron-phonon interaction on the single-particle spectral function and the optical absorption spectrum. The dynamical DMRG data are compared with experimental data of 1D copper oxide Mott insulators.

§1. Introduction

The interplay of strong electron-electron correlation and electron-phonon (EP) interaction has recently attracted much attention.[1)] One of the issues is to understand the effect of the EP interaction on carriers introduced into a Mott insulator. In the ground state of the Mott insulator, the on-site Coulomb repulsion makes the charge distribution uniform, and then the EP interaction is irrelevant. However, the mobile carriers created in the Mott insulator by chemical and/or photo dopings induce the charge fluctuation, and thus the EP interaction is expected to play an important role in various physical quantities.[2)–9)]

The charge gap in Mott insulators is a consequence of strong electron correlation represented by large on-site Coulomb interaction. The correlation induces novel phenomena in terms of the interplay of charge and spin degrees of freedom.[10)] In one-dimensional (1D) Mott insulators, two particles created by photo-excitation, i.e., an unoccupied site and a doubly occupied site of electrons, can move inside the system without being disturbed by surrounding spins in the background. This is a manifestation of a separation of the charge and spin degrees of freedom, called the spin-charge separation inherent in 1D correlated electron systems. Optical responses in the 1D Mott insulators are characterized by this phenomenon.[11)–14)] Therefore, it is interesting whether the decoupling of spin and charge degrees of freedom is robust or not in the presence of the EP interaction. This issue has been discussed by examining the spectral function of the Hubbard-Holstein model.[7),8)]

The nature of the two particles in the photoexcited states is obtained by examining the linear susceptibility $\chi^{(1)}$ with respect to the applied electric field, which provides information on the dipole-allowed states with odd parity among the photoexcited states. In addition to $\chi^{(1)}$, the third-order nonlinear optical susceptibility

*) E-mail: tohyama@yukawa.kyoto-u.ac.jp
**) E-mail: matsueda@cc.sendai-ct.ac.jp

$\chi^{(3)}$ is useful to detect not only the odd-parity states but also the dipole-forbidden states with even parity.[15] Recently, large values of $\chi^{(3)}$ have been reported for 1D Mott insulators of copper oxides such as Sr_2CuO_3[16),17] from the electro-reflectance measurement[16] and the pump and probe spectroscopy.[17] The analyses of $\chi^{(3)}$ have suggested that odd- and even-parity states are nearly degenerate with a large transition dipole moment between them. Theoretically, $\chi^{(3)}$ in the 1D Mott insulators has been examined by employing the numerically exact diagonalization technique for small clusters of the Hubbard model at half filling.[13] It has been shown that odd- and even-parity states are almost degenerate in the same energy region and that the degeneracy is due to the spin-charge separation and strong on-site Coulomb interaction.[18]

In the realistic parameter range of Sr_2CuO_3, there is an exciton that is a pair of two particles, called holon and doublon, formed by long-range Coulomb interactions.[19),20] The exciton may be influenced by the EP interaction, since it has charge fluctuation, in contrast to uniform charge distribution of the spin background. The shape of the exciton peak is expected to be strongly dependent on the interaction. However, there are only a few works on the relation between the exciton in the 1D Mott insulator and electron-phonon interaction.[21),22] In addition to the exciton, the relaxation process of the photo-excited states in the Mott insulator may be affected by the EP interaction as is the case of the exciton of semiconductors. This would be reasonable since the spin degrees of freedom is expected to be separated from the charge and thus direct coupling between charge and phonon may contribute to the relaxation process. In 1D Mott insulators, it has been demonstrated that the relaxation time to the original state before photoexcitation is ultra fast with a few pico seconds. By combining the ultra fast relaxation and the large $\chi^{(3)}$, the 1D Mott insulators are expected to be available for optical switching devices in the future. Therefore, inclusion of the phonon degree of freedom is inevitable when one tries to fully understand photoexcitation phenomena in the 1D Mott insulators and to form the basis for the future optical devices.

The effect of the EP interaction on the optical responses has also been an important topic in the physics of high-temperature superconductors with two-dimensional CuO_2 plane. There are several theoretical works on this topics in terms of angle-resolved photoemission spectroscopy (ARPES)[23)–25] and optical conductivity.[26] It is also interesting how the difference of dimensionality influences on the effect of the EP interaction.

In order to calculate dynamical properties in 1D strongly correlated electron systems, a dynamical version of the density-matrix renormalization group (DMRG) is very powerful.[27)–33] In this paper, we will address the effect of EP interaction on optical properties in the 1D Mott insulators, based on the dynamical DMRG study of the Hubbard-Holstein model at half filling. In particular, we will focus on the single-particle spectral function[8] and the optical absorption.[22] We find that the single-particle spectral function is nicely interpreted by a simple superposition scheme of spectra for a spinless carrier dressed with phonons. The superposition is a consequence of robustness of the decoupling of spin and charge degrees of freedom against electron-phonon coupling. The optical absorption spectrum exhibits

a peculiar behavior that the effect of the electron-phonon interaction on an exciton is enhanced by increasing the on-site Coulomb repulsion. Phonon-assisted spin excitation in the absorption spectrum is also investigated.

This paper is organized as follows. In §2, we introduce the Hubbard-Holstein model and the dynamical DMRG to calculate the single-particle spectral function and the current-current correlation function. In §3, the effect of the EP interaction on the spectral function at half filling is discussed. It will be shown that the concept of the wavefunction factorization between the spin and charge components manifests even in the presence of the EP interaction. The current-current correlation function is calculated in §4 and the relation between the strength of the on-site Coulomb interaction and the EP interaction is discussed. The presence of phonon-assisted spin excitations in the Hubbard-Holstein model is also demonstrated. A summary is given in §5.

§2. Model and method

The Hubbard-Holstein model is a basic model to study the interplay between electron correlation and EP coupling in cuprates.[34),35)] In order to examine physical properties in the 1D Hubbard-Holstein model, we use dynamical DMRG technique, which gives accurate numerical results for a given lattice.

2.1. *Hubbard-Holstein model*

The coupling between an electron and breathing phonons in the cuprates can be mapped onto the Holstein- and Peierls-type interactions.[35)] Since the Holstein interaction is stronger than the Peierls one, we consider the Hubbard-Holstein model in one dimension. In addition, we introduce the nearest neighbor Coulomb repulsion which leads to an exciton. The Hamiltonian is defined by

$$H = -t\sum_{i,\sigma}(c^{\dagger}_{i,\sigma}c_{i+1,\sigma} + \text{H.c.}) + U\sum_{i} n_{i,\uparrow}n_{i,\downarrow} + V\sum_{i}(n_i - 1)(n_{i+1} - 1) \\ +\omega_0\sum_{i} b^{\dagger}_{i}b_i - g\sum_{i}(b^{\dagger}_{i} + b_i)(n_i - 1), \tag{2·1}$$

where $c^{\dagger}_{i,\sigma}$ ($c_{i,\sigma}$) is a creation (annihilation) operator of an electron at site i with spin σ, and $b^{\dagger}_{i}$ (b_i) is a creation (annihilation) operator of a phonon at site i. This model includes electron hopping, t, on-site and nearest-neighbor Coulomb repulsions, U and V, respectively, phonon frequency, ω_0, and EP coupling, g. Here, we neglect the dispersion of the phonon in order to make our discussion simple. Keeping cuprates in mind, we take U larger than the band width $4t$. Here, we briefly mention how to construct the model Hamiltonian in the case of the cuprates. The lower Hubbard band of (2·1) corresponds to the Zhang-Rice singlet which is derived from a three-band model for Cu $3d_{x^2-y^2}$ and O $2p$ orbitals with lattice distortion. The distortion leads to changes of the hopping integral of an electron between neighboring Cu and O orbitals. Due to the modulation of the hopping integral, the diagonal (Holstein) term dominates in the effective Hamiltonian for the Zhang-Rice singlet in comparison

with off-diagonal (Peierls) terms.[34),35)]

In (2·1), we have introduced the V-term, $V(n_i-1)(n_{i+1}-1)$, instead of the standard notation, Vn_in_{i+1}. The present term prevents the localization of unoccupied state (holon) and doubly occupied state (doublon) at the edge under open boundary conditions, and thus reduces a boundary effect.

2.2. *Dynamical DMRG*

We apply the dynamical DMRG method to the calculation of the dynamical quantity in terms of an operator A given by

$$I(\omega) = -\frac{1}{\pi}\mathrm{Im}\left\langle 0 \left| A^\dagger \frac{1}{\omega - H + E_0 + i\gamma} A \right| 0 \right\rangle, \tag{2·2}$$

where $|0\rangle$ denotes the ground state with energy E_0, and γ is a small positive number. We introduce a mixed-state density matrix which is composed of the ground state $|0\rangle$, an excited state $A|0\rangle$, and $N_{\rm cv}$ correction vectors $|\epsilon\rangle \equiv (\epsilon + E_0 - H + i\gamma)^{-1}A|0\rangle$ with $\epsilon = \omega$, $\omega+2\gamma$, $\omega+4\gamma$, ..., $\omega+2(N_{\rm cv}-1)\gamma$. By using these states simply denoted by $|\psi_n\rangle$ with $n = 1$, 2, ..., $N_{\rm cv}+2$, the density matrix of the system (or environment) block is defined by $\rho = \mathrm{Tr}\sum_n p_n |\psi_n\rangle\langle\psi_n|$, where $\sum_n p_n = 1$ and the trace is taken for the environment (or system) states. We call $|\psi_n\rangle$ target states. When $N_{\rm cv} = 2$, we have four target states: $|\psi_1\rangle = |0\rangle$ (obtained by the Lanczos method), $|\psi_2\rangle = A|0\rangle$, $|\psi_3\rangle = |\omega\rangle$, and $|\psi_4\rangle = |\omega+2\gamma\rangle$. The weight p_n is taken to be equal for all the target states in our calculations. We note that this choice is less sensitive to the spectral weight. As a result, the mixed-state density matrix ρ contains information on not only the ground state but also excited states contributing to the spectrum through $|\psi_n\rangle$ ($n > 1$). The spectral weight (2·2) for the range of $\omega < \epsilon < \omega + 2(N_{\rm cv}-1)\gamma$ is calculated after one DMRG run using ρ. The number of the eigenstates of ρ retained for the next DMRG step is called the truncation number m. When we can take sufficiently large m, it is possible to increase $N_{\rm cv}$ and scan a wide energy range in one DMRG run. Usually, we take $N_{\rm cv} = 2$, but in some cases we take much larger $N_{\rm cv}$, although we need larger m as expected. It is technically useful to note that good numerical convergence is obtained when $I(\omega)$ for $\omega_1 < \epsilon < \omega$ is smoothly connected with that for $\omega < \epsilon < \omega_2$. Further, we comment on why the two targets for ω and $\omega+2\gamma$ guarantee the precision of the spectra inside them. For this purpose, we take an inner product between $|\omega\rangle$ and $|\omega+2\gamma\rangle$, leading to

$$\langle\omega\,|\omega+2\gamma\rangle = \sum_n \frac{|\langle 0|\,A\,|0\rangle|^2}{(\omega+\gamma+E_0-E_n)^2 + 2\gamma(\omega+E_0-E_n)i}, \tag{2·3}$$

for small γ. This means that the inner product is relatively large for $E_n - E_0 \sim \omega+\gamma$. Thus, the information for $|\epsilon\rangle$ around $\epsilon \sim \omega+\gamma$ can be renormalized by these targets.

In the present study, the correction vector $|\omega\rangle = (\omega + E_0 - H + i\gamma)^{-1}A|0\rangle$ is calculated by a modified version of the conjugate gradient method. This method is powerful, but becomes slow when γ is less than $0.1t$. When we need to take γ of the order of $0.01t$, it is better to expand $|\omega\rangle$ in terms of approximate eigenstates of the Hamiltonian constructed by the Lanczos iteration. In the following, we explain this

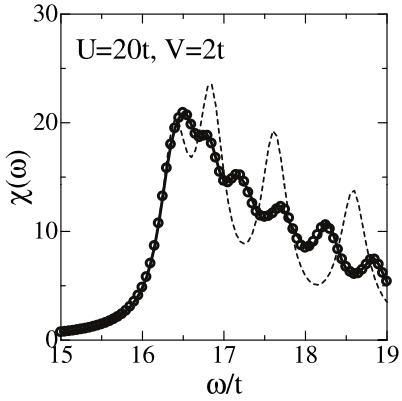

Fig. 1. $n_{\rm LV}$ dependence of the current-current correlation function $\chi(\omega)$ for the extended Hubbard model with $U = 20t$ and $V = 2t$. We take $L = 20$, $n_{\rm LV} = 100$ (dashed line, $m = 300$), 200 (solid line, $m = 300$), and 400 (open circles, $m = 400$).

approach. By using a complete set $\{|n\rangle\}$, the correction vector is expanded by the following form,

$$|\omega\rangle = \sum_n |n\rangle \frac{1}{\omega + E_0 - E_n + i\gamma} \langle n| A |0\rangle . \tag{2·4}$$

We replace $|n\rangle$ with $|\tilde{n}\rangle$ obtained by using the Lanczos procedure. The dimension of $|\tilde{n}\rangle$ is at most the order of 1000, which is determined by the number of the Lanczos step. The reduction of the Hilbert space is a major approximation of this approach. Here, we take $A|0\rangle$ as an initial vector of the Lanczos iteration in order to create a set of vectors, $\{|u_i\rangle\}$, for the tri-diagonal Hamiltonian matrix. This matrix is easily diagonalized by a transformation matrix v. Since we have relations, $v_{1,n} = \langle\tilde{n}| A |0\rangle$ and $|\tilde{n}\rangle = \sum_i v_{i,n} |u_i\rangle$, $|\omega\rangle$ can be approximately described by

$$|\omega\rangle \sim \sum_n \sum_i \frac{v_{i,n} v_{1,n}}{\omega + E_0 - \tilde{E}_n + i\gamma} |u_i\rangle , \tag{2·5}$$

where $\tilde{E}_n$ is the approximate eigenvalue given by the Lanczos method. It is noted that the state $|u_i\rangle$ has a dimension of the original superblock Hamiltonian, and thus we can go to further numerical steps. The number of the Lanczos step, $n_{\rm LV}$, required for realistic calculations are ranged from 100 to 1000 depending on the energy scale. We show one example of numerical convergence in Fig. 1, where the current-current correlation function of the extended Hubbard model (20-site chain with $U = 20t$ and $V = 2t$) is shown. In this case, the convergence is almost discontinuous as a function of $n_{\rm LV}$, and then it is easy to check the reliability of calculation. We found that high-energy structures beyond the charge gap are described by relatively small Lanczos steps, while low-energy spin excitations require the order of 1000 iterations. This is because in early steps of the Lanczos iteration, the eigenstates sparsely distribute at wide energy range, and then the sparseness is lost by further iterations because of inclusion of low-energy excitations.

The treatment of infinite bosonic degrees of freedom is one of important topics in numerical simulations. Here, we use two methods. One is that the original single site is divided into fermionic and phononic sites, and the phonon sites are directly treated. In this case, the phonon states per site, M, can be truncated up to 32 sites. The other one is the pseudo-boson method, where a boson operator with a restricted Hilbert space is exactly transformed into a set of N hard-core bosons, namely $M = 2^N$. For instance, the boson operator with $M = 4$ is transformed into

$$b^\dagger = a_1^\dagger + \sqrt{2}a_2^\dagger a_1 + (\sqrt{3} - 1)a_1^\dagger a_2^\dagger a_2 \tag{2·6}$$

with use of the two ($N = 2$) hard-core boson operators, a_1 and a_2. Then, step-by-step renormalization of each boson is carried out. We have taken up to $N = 4$ hard-core bosons. We have checked consistency between the two methods.

In this paper, we examine two dynamical quantities. One is the electron-removal single-particle excitation spectrum $A(k, \omega)$ at zero temperature that is given by replacing the operator A in (2·2) with an annihilation operator of an electron with momentum k and up spin, $c_{k,\uparrow}$ and by changing ω to $-\omega$. $A(k, \omega)$ is calculated by the finite-system DMRG algorithm. Since the nearest-neighbor Coulomb repulsion V has no net effects on $A(k, \omega)$ at half filling, we set $V = 0$. In this case, in order to reduce boundary effects under the open boundary conditions, we introduce a potential $-tn_i$ at the edges. We note that the momentum k is defined by $k = n\pi/(L + 1)$ with $n = 1, 2, ..., L$ under the open boundary conditions. The momentum representation of $c_{l,\uparrow}$ is, thus, given by $c_{k,\uparrow} = \sqrt{2/(L + 1)} \sum_l \sin(kl) c_{l,\uparrow}$.[31] The system size L is taken to be 20 lattice sites. It is noted that the spectrum for $L = 20$ is similar to that for $L = 120$ without the edge potential. The DMRG bases are truncated up to $m = 400$ states from the density matrix during finite-system DMRG processes.

We also examine the current-current correlation function $\chi(\omega)$ that is given by replacing A in (2·2) with the current operator j. The current operator j is defined by

$$j = -it \sum_{i,\sigma} (c_{i,\sigma}^\dagger c_{i+1,\sigma} - \text{H.c.}). \tag{2·7}$$

The optical absorption spectrum is proportional to $\chi(\omega)/\omega^2$. In order to calculate $\chi(\omega)$, the infinite-system DMRG method[27] is applied to an open boundary system. We have also carried out the finite-system DMRG calculation for some data, and this calculation quantitatively agrees with the infinite-system DMRG data. The truncation number m is taken to be $m = 300$.

§3. Single-particle spectral function

It is well-known that the electron-removal spectral function in an 1D Mott insulator shows two branches characterized by a spinon and a holon. This is one of characteristics of the emergence of the spin-charge separation, and has been observed in, for example, 1D cuprates like $SrCuO_2$.[37] Figure 2(a) shows the dynamical DMRG result of $A(k, \omega)$ in the 1D half-filled Hubbard model ($U = 10t$ and $V = 0$)

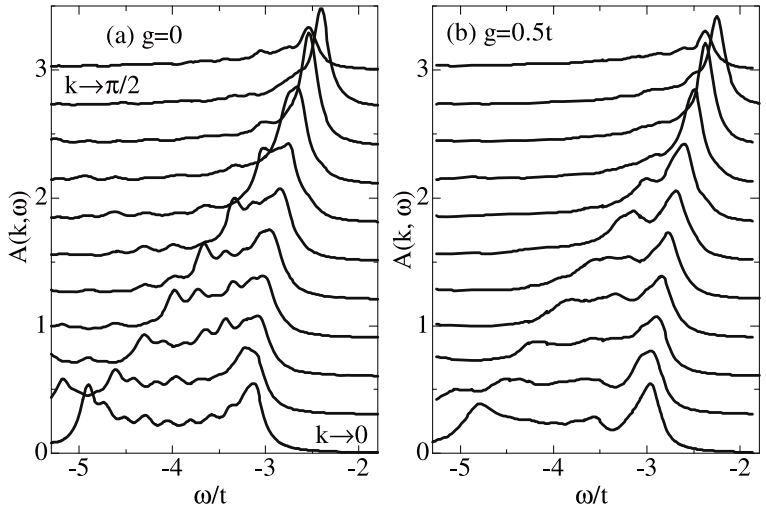

Fig. 2. $A(k,\omega)$ for the 1D Holstein-Hubbard model at half-filling with $U = 10t$ and $V = 0$. (a) $g = 0$. (b) $g = 0.5t$ and $\omega_0 = 0.5t$. The momentum is taken from $\pi/21$ to $11\pi/21$.

without the EP coupling ($g = 0$). γ in (2·2) is taken to be $\gamma = 0.1t$, which is small enough to resolve spinon dispersion of the order of the exchange interaction $J \sim 4t^2/U = 0.4t$ as well as phonon structures with the energy scale of ω_0 set to be $0.5t$ below. The origin of energy is located at the center of the Mott gap. A single peak at $k \sim \pi/2$ separates to two branches toward $k \sim 0$. These energy positions are $\omega/t = -3.13$ and -4.90 at $k = \pi/21$, which is the minimum momentum in the calculation. The branch located in low (high) binding energy side is deduced to be the spinon (holon) branch. Here, fine structures inside the branches come from the finite size effect.

The presence of the two branches in the electron-removal spectral function of a large U Hubbard model is qualitatively explained based on the Bethe anzats solution[38] at large U limit. In this limit, the wave function of all eigenstates can be decomposed into the product of two wave functions representing the spin and charge parts.[39] The electron-removal spectral function is constructed by superposition of a set of holon dispersions forming a cosine band with the width of $4t$.[40] The shaded area in Fig. 3(a) exhibits the region where the spectral weight exists.

The superposition is a consequence of the spin-charge separation, because each of the holon dispersions is characterized by one spinon momentum. Therefore, an effective model of the spectral function, $A_{\rm eff}(k,\omega)$, is constructed by putting the spectral weight for a spinless fermion, $A_h(p,\varepsilon) = \delta(\varepsilon - 2t\cos p)$, on each of the holon dispersions. Since a top of the cosine band is running along the spinon dispersion $\varepsilon_s(q+\pi/2) = -(\pi J/2)|\sin(q+\pi/2)|$ for $-\pi/2 \le q \le \pi/2$ (the upper-left edge of the shaded area in Fig. 3(a)) with $J = 4t^2/U$, $A_{\rm eff}(k,\omega)$ is defined by

$$A_{\rm eff}(k,\omega) = \sum_{q=-\pi/2}^{\pi/2} A_h\left(k-q, \omega + 2t + \varepsilon_s\left(q+\frac{\pi}{2}\right)\right), \qquad (3\cdot1)$$

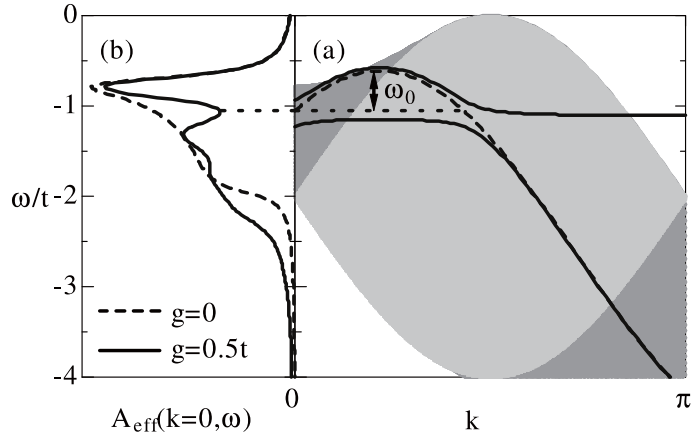

Fig. 3. (a) Shaded area represents the region where $A(k,\omega)$ is finite in a 1D Mott insulator. The darker the color is, the larger the weight is. Dashed (solid) line denotes a holon dispersion for $g=0$ ($g\neq 0$). A dotted line is for a guide to the eye. (b) $A_{\rm eff}(k=0,\omega)$. Dashed (solid) line is for the case of $g=0$ ($g=\omega_0=0.5t$). A broadening $\gamma=0.1t$ is assumed.

except for constant energy shift. A dashed line in Fig. 3(b) shows $A_{\rm eff}(k=0,\omega)$. The singularity of the spinon branch appears at $\omega=-\pi J/2\sim -2\pi t^2/U=-0.785t$. The singularity comes from the flatness of the spinon dispersion near $k=0$. The lineshape is consistent with the dynamical DMRG data in Fig. 2(a) except for the singularity of the holon branch. The singularity of the holon branch is explained by taking into account the phase string effect[41] that is not included in (3·1).

Let us introduce the EP coupling. Figure 2(b) shows $A(k,\omega)$ at $g=0.5t$ and $\omega_0=0.5t$. We find that the holon branch becomes broad due to the EP coupling, while the spinon branch remains sharp. We also find a 'peak-dip-hump' structure at the high-binding energy side of the spinon branch. The dip disperses followed by the spinon branch.

In order to investigate the origin of the dip, the ω_0 and g dependence of $A(k,\omega)$ at $k\rightarrow 0$ is shown in Fig. 4. The energy of the dip (hump) position decreases with increasing ω_0. The energy difference between the dip (hump) and the spinon branch is estimated to be ω_0, which means that the peak-dip-hump structure is due to the phonon effect. Therefore, the origin of the peak-dip-hump structure provides information on the effect of phonon. As g goes from $0.5t$ to larger values with keeping $\omega_0=0.5t$, the spinon branch starts to broaden as seen in Fig. 4(b). The weight of the spinon branch decreases linearly as a function of g for $g\geq\omega_0$. For $g=t$, the holon branch is completely smeared out. The peak-dip-hump structure observed in Fig. 2(b) develops into multipeaks whose positions are $\omega/t=-3.13$, $-3.61\simeq -3.13-\omega_0$, and $-4.09\simeq -3.13-2\omega_0$. Furthermore, a slight enhancement of the low-binding energy side of the spinon branch is seen. The energy difference between the enhancement and the band top ($k=\pi/2$) for $g=0$ is estimated to be ω_0. Therefore, the three main peaks and the enhancement are also due to the electron-phonon coupling.

In order to understand the calculated data, we first introduce a working hypoth-

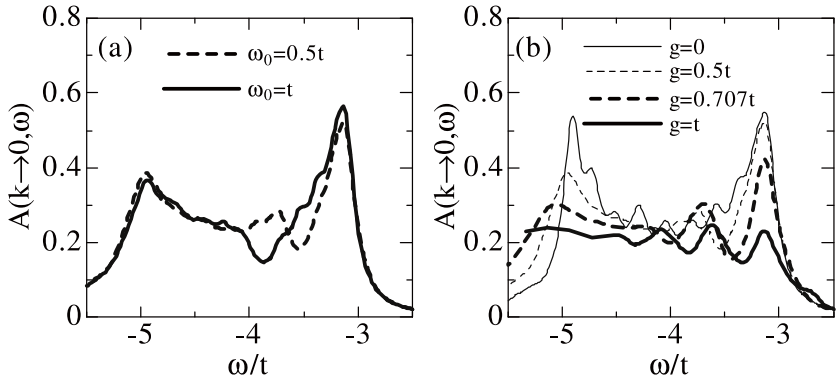

Fig. 4. $A(k,\omega)$ at $k \to 0$. (a) ω_0 dependence keeping $g = 0.5t$, and (b) g dependence keeping $\omega_0 = 0.5t$. The spectra with $g \neq 0$ are shifted so that the energy of the spinon branch is taken to be equal.

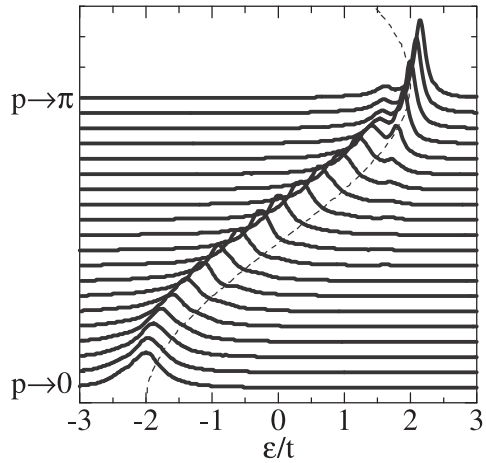

Fig. 5. Single-particle spectral function $A_h(p-\pi,\varepsilon)$ for the 1D Holstein model, i.e. a model for a spinless carrier coupled with Einstein phonons ($g = \omega_0 = 0.5t$). A dashed line is a cosine band with the width $4t$.

esis that the decomposition of the wave function into the spin and charge parts, i.e., the decoupling of spin and charge, is still holding even in the presence of the EP coupling. This hypothesis leads to the effective electron-removal spectral function (3·1). $A_h(p,\varepsilon)$ in this case, however, is not of a spinless free fermion, but of a spinless fermion dressed with Einstein phonons. Figure 5 shows such a dispersion calculated for an 1D Holstein model with $g = \omega_0 = 0.5t$. The calculated $A_h(p-\pi,\varepsilon)$ splits into low-lying peaks and an incoherent part.[42)–45)] The splitting occurs at the anticrossing point $\varepsilon \sim 1.5t$ that is away from the top of the band ($p = \pi$) by ω_0. At $\varepsilon \sim 1.5t$, we find a tiny spectral weight with a flat dispersion coming from the phonon branch.

A dispersion with such a splitting seen in Fig. 5 is schematically plotted in Fig. 3(a). $A_{\rm eff}(k=0,\omega)$ constructed from the dispersions is shown by a solid line in Fig. 3(b). A peak-dip-hump structure clearly appears. The spectral weight lost by the dip is transferred to a high-energy region. We find that the peak-dip-hump struc-

ture obtained by using (3·1) is qualitatively consistent with the dynamical DMRG data, indicating the justification of the working hypothesis. In other words, the decoupling of spin and charge is robust against the EP coupling.[8)]

The data shown in Fig. 4(b) for $g \geq \omega_0$ indicate the decrease of the spectral weight of the spinon branch. As mentioned above, the spinon branch can be expressed by the superposition of the peak at $\omega \sim 2t$ in Fig. 5. It has been shown that the spectral weight of the peak decreases with increasing g.[42)–45)] Therefore, the weight of the spinon branch decreases with increasing g. The multi-peak structure as well as the slight enhancement of the low-binding energy side of the spinon branch for $g = t$ in Fig. 4(b) is also explained by the effective model (3·1).[8)]

Since the spectral weights obtained from (3·1) give reasonable interpretations for the dynamical DMRG results, the working hypothesis that the decoupling of spin and charge is present under the EP coupling seems to be justified. The robustness of the decoupling leads to a difference between 1D and 2D systems in terms of the interplay of strong electron correlation and EP coupling.[8)] In order to see the difference, we introduce a dimensionless parameter $\lambda = g^2/\omega_0 W$ with the noninteracting band width W. There is a characteristic λ value, λ^*.[46)] For $\lambda < \lambda^*$, the lowest energy excitation is weakly dressed with phonons. As λ approaches to λ^*, the excitation loses its weight rapidly. Then, the dominant low-energy excitation moves to a heavily dressed polaron. In the 1D Holstein model, λ^* is estimated to be $\lambda^* \sim 1$.[47),48)] In the 1D Hubbard-Holstein model, the spinon branch loses its weight for $\lambda^* \sim 1$ ($g^* \sim 1.4t$) as estimated from Fig. 4(b). This is because the spinon branch can be expressed by the superposition of the spectra for the low-energy excitation of the Holstein model. In 2D, on the other hand, λ^* is close to 0.2 in the t-J-Holstein model with $J = 0.3t$, while $\lambda^* > 0.6$ in the Holstein model.[2),23),49)] This means that the AF correlation helps the formation of the lattice polaron.[4),50),51)]

Finally, let us discuss the ARPES data for a 1D Mott insulator $SrCuO_2$ in the light of the dynamical DMRG data. In this compound, high-energy ARPES experiments have been done, where the spinon and holon branches were observed.[37)] Near the Γ point, the intensity of the holon branch is smaller than that of the spinon branch. In addition, these branches do not exhibit singularities predicted by the Hubbard model.[40)] The dynamical DMRG data appropriate for 1D cuprates is shown in Fig. 4(b) with $\lambda = 0.25$[35)] ($g = 0.707t$ and $\omega_0 = 0.5t$). The calculated data is qualitatively consistent with the ARPES data except for the presence of the dip. The dip may be washed away by the phonon dispersion or smeared out due to finite-temperature effects.

§4. Current-current correlation function

In this section we examine the current-current correlation function that is related to the optical absorption spectrum. We focus on both high-energy charge excitation across the Mott gap and low-energy excitations inside the Mott gap.

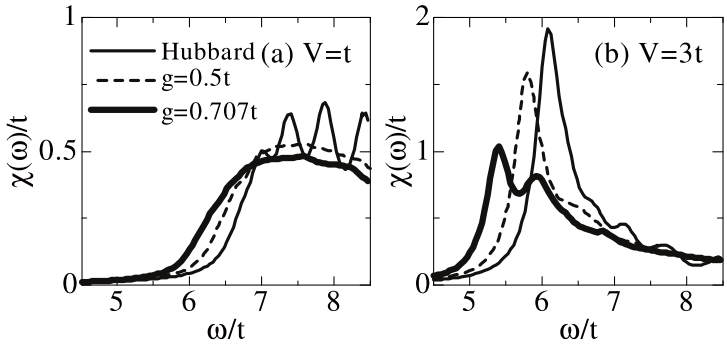

Fig. 6. g dependence of current-current correlation function $\chi(\omega)$ for the 20-site half-filled Hubbard-Holstein model with $U = 10t$. (a) $V = t$ and (b) $V = 3t$.

4.1. *High-energy charge excitations*

Figure 6 shows $\chi(\omega)$ in the energy region of Mott-gap excitations for various g and V values of a half-filled Hubbard-Holstein model. We take $L = 20$, $U = 10t$, and $\omega_0 = 0.5t$. The broadening factor is set to be $\gamma = 0.2t$, which is larger than the case of the spectral function but still smaller than J and ω_0. We note that, the larger the value of γ is, the shorter computational time is. The magnitude of ω_0 may be three-times larger than the frequency of the breathing mode in cuprates.[35)]

For $g = 0$, the V dependence of the spectra has been studied intensively, and the present data are consistent with the previous data:[52)] for $V < 2t$ only a continuum band exists, which is composed of nearly free holon and doublon, while for $V \geq 2t$ the holon and doublon form an excitonic bound state. A pronounced peak at $\omega = 6.1t$ in Fig. 6(b) corresponds to the exciton. Note that the spiky structures in Fig. 6(a) come from the finite-size effect.

The effect of the EP interaction on the exciton is larger than that on the continuum band. For $V < 2t$ and $g > 0$, the continuum band edge shifts toward lower-energy region. This is because the holon and doublon are dressed with phonons, leading to an energy gain of the photoexcited state. The second-order perturbation expansion with respect to g for $t = 0$ gives an effective reduction of U by $2g^2/\omega_0$. However, the shift in the DMRG data is smaller than $2g^2/\omega_0$. For instance, the energy gain for $V = t$ and $g = \sqrt{0.5}t$ in Fig. 6(a) is about $0.5t$, and this is smaller than $2g^2/\omega_0 = 2t$. In this sense, we can say that the motion of holon and doublon suppresses the effect of the EP coupling in the region of $V < 2t$.

For $V \geq 2t$ and $g > 0$, the exciton peak splits into multiple peaks. For $g = \sqrt{0.5}t$ in Fig. 6(b), these peaks are positioned at $5.38t$ and $5.85t$. The energy difference between them is $0.47t \sim \omega_0$, and thus it is expected that the exciton has a polaronic feature. Because of the splitting, the line shape of the exciton is asymmetric. The shape is different from that obtained by a classical treatment of phonons.[21)] The energy gain of the exciton by g is still smaller than $2g^2/\omega_0$, even though the exciton would be localized for $V = 3t$.

Next, we examine whether the effect of g on the exciton is enhanced or reduced by U. For this purpose, we compare the spectra for $U = 10t$ and $20t$. It is usually

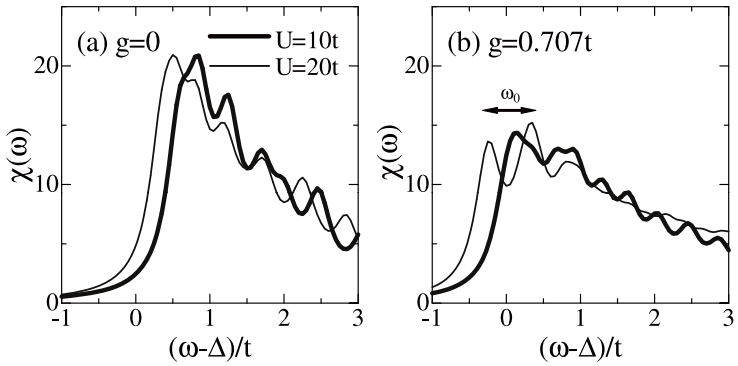

Fig. 7. Current-current correlation function $\chi(\omega)$ for the 20-site half-filled Hubbard-Holstein model with $V = 2t$. $U = 10t$ and $U = 20t$. (a) $g = 0$ and (b) $g = 0.707t$. The energy ω is shifted by $\Delta = U - V - 4t^2/V$.

recognized that the parameter $U = 10t$ is characteristic of strong electron-electron correlation. Actually, for $g = 0$, the absorption spectra for these parameters are almost the same. However, the line shape of the stress tensor correlation function, i.e., the correlation with respect to an operator $\tau = t\sum_{i,\sigma}(c^{\dagger}_{i,\sigma}c_{i+1,\sigma} + \text{H.c.})$, changes dramatically even for $10t < U < 40t$.[52] As will be shown later, we can see quantitative difference between the absorption spectra for $U = 10t$ and $20t$ in the presence of g. This means that the effect of g on the spectra is sensitive to the value of U.

Figure 7 shows comparison of $\chi(\omega)$ between $U = 10t$ and $20t$. Here, V is taken to be $2t$, and thus the lowest-energy photoexcited state is an exciton. We take $m = 300$ and $n_{\rm LV} = 100 \sim 200$. All of the correction vectors are targeted in one DMRG run. In the figure, the energy ω is shifted by $\Delta = U - V - 4t^2/V$ for comparison. When $g = 0$, the two spectra are almost the same, while in the presence of g, the qualitative difference of their lineshapes appears at the low-energy edge: the spectral weight of the lowest-energy peak is largest for $U = 10t$, while the weight of the lowest-energy peak is smaller than that of the second-lowest-energy peak in the case of $U = 20t$. Therefore, the increase of U significantly changes the lineshape of the exciton in the presence of g. This means that the effective electron-phonon coupling increases with U.

Let us consider why U enhances the effect of the EP interaction on the exciton.[22] First of all, it would be useful for later discussion to introduce the exactly solvable case of the holon-doublon model corresponding to $U \to \infty$. In the large-V limit, using a canonical transformation,[53] we have the following result:

$$\chi(\omega) = -\frac{1}{\pi L}\mathrm{Im}\sum_{l=0}^{\infty}\frac{A_l}{\omega - \Omega_l + i\gamma}, \tag{4·1}$$

with $A_l = 8\pi(2g^2/\omega_0^2)^l \exp(-2g^2/\omega_0^2)/l!$ and $\Omega_l = U - V - 4t^2/V - 2g^2/\omega_0 + l\omega_0$. We find that the spectral weight for the lowest-energy photoexcited state $|n_0\rangle$, $A_0 = 8\pi\exp(-2g^2/\omega_0^2)$, decreases exponentially as g increases. On the other hand, the decrease of the spectral weights for higher-energy photoexcited states $|n_l\rangle$ is

suppressed by a factor $(2g^2/\omega_0^2)^l$. When $g > \omega_0/\sqrt{2}$, A_0 becomes smaller than A_1 because of strong renormalization of $|n_0\rangle$ due to large EP coupling. In this case, we expect large expectation value of the phonon number for $|n_0\rangle$, $N_0 = \langle n_0| \sum_i b_i^\dagger b_i |n_0\rangle$. In the following consideration, we assume this parameter region where $|n_0\rangle$ is strongly renormalized and $A_0 < A_1$. In the large-U limit, $|n_0\rangle$ is composed of the bases with one holon-doublon pair. As a result, phonons are spontaneously excited around the pair, leading to large N_0. On the other hand, when U decreases, the bases without the pair enter into $|n_0\rangle$. Since these bases represent homogeneous charge distribution, N_0 decreases as U decreases.

Next, we examine A_0 as a function of N_0 in order to understand the relation between A_0 and U. It is clear that the dominant contribution to the ground state comes from $|0\rangle \sim |AF\rangle\,|0)$, where $|AF\rangle$ and $|0)$ represent the antiferromagnetic state and phonon vacuum, respectively, as long as the ground state is the Mott insulator. In this case, $A_0 = |\langle n_0|\, j\, |0\rangle|^2$ is given by

$$A_0 \sim \left| t \sum_i \langle n_0| \left(|0, \uparrow\downarrow\rangle_{i,i+1} - |\uparrow\downarrow, 0\rangle_{i,i+1} \right) |0) \right|^2 , \tag{4·2}$$

where the holon-doublon pair $|0, \uparrow\downarrow\rangle$ is located on the i-th and $(i+1)$-th sites. This equation shows the relation between A_0 and N_0. When N_0 decreases, the weights of the bases without phonons become dominant in $|n_0\rangle$, and this effect increases A_0. According to the previous paragraph where we found that N_0 decreases with decreasing U, A_0 increases with decreasing U. We have also confirmed U dependence of N_0 and A_0 by exact diagonalization on small clusters. Therefore, we can conclude that the effect of the EP interaction on an exciton is very strong in 1D Mott insulators.

Let us compare the present DMRG results with the optical absorption spectrum in the 1D cuprate Sr_2CuO_3.[54] The absorption spectrum has asymmetric structure: the high-energy side of the spectrum is broad, while the low-energy side is fitted with a single Lorentzian function with a broadening factor of the order of 0.1 eV. In addition, a flat part at the top of the absorption peak is seen ($1.75\text{eV} \lesssim \omega \lesssim 1.82\text{eV}$). The energy range 0.07 eV of this flat part is comparable to a phonon frequency of the breathing mode seen in $Ca_{1.8}Sr_{0.2}CuO_3$.[55] We consider that the flat part is a signature of multiple phonon peaks, although the clear peak structures would be washed away by the phonon dispersion.

4.2. *Low-energy spin excitations*

Optical processes usually couple with the charge degrees of freedom. However, once one introduces the EP coupling, spin excitations can appear in the optical processes via lattice deformation. The excitations inside the Mott gap have been discussed theoretically[56] and observed experimentally[57] in the 1D Mott insulator Sr_2CuO_3. The observed low-energy excitation in the optical conductivity has been interpreted as spinon excitations.[57),58] The interpretation is based on the analyses of the Heisenberg model to which a matrix element of the dipole transition coming from the EP coupling is taken into account. Thus, it seems to be important to check whether the Hubbard-Holstein model itself produces or not the phonon-assisted

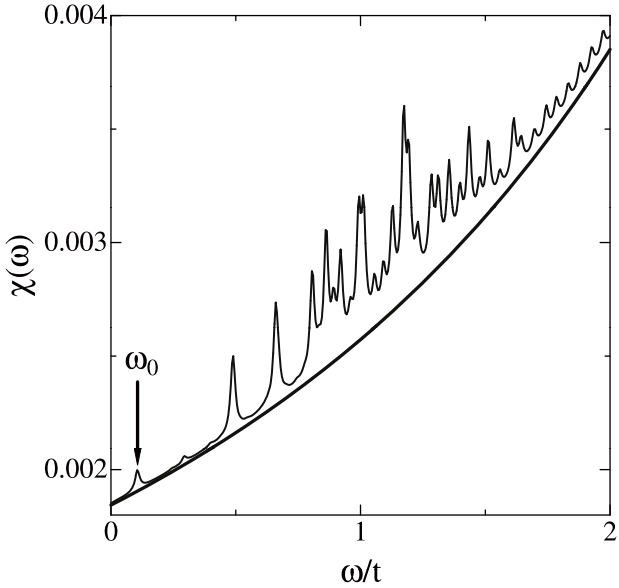

Fig. 8. Phonon-assisted spin excitations seen inside of the charge gap in $\chi(\omega)$ for the 12-site half-filled Hubbard-Holstein model with $U = 10t$ and $V = 3t$. Fine and bold solid lines denote $\chi(\omega)$ with and without g, respectively. $g = 0.25t$, $\omega_0 = 0.1t$, and $\gamma = 0.01t$.

spinon excitations in the optical absorption. In order to investigate this, we need to be careful of the magnitude of ω_0. Since we are interested in the low-energy region where spinon excitations occur, the relative magnitude of ω_0 and exchange interaction J is a crucial parameter. We take $J \sim 0.4t > \omega_0 \sim 0.1t$ for the analysis of Sr_2CuO_3.

Figure 8 shows low-energy excitations in $\chi(\omega)$. Parameters are set to be $U = 10t$, $V = 3t$, $g = 0.25t$, and $\omega_0 = 0.1t$, which satisfies $J \sim 4t^2/(U - V - 4t^2/V) > \omega_0$. We take $L = 12$, $m = 400$, and $\gamma = 0.01t$. We need a small value of γ compared with previous values ($0.1t \sim 0.2t$) since the value of ω_0 in this calculation is small. All of the correction vectors with $0 \leq \omega \leq 2t$ are targeted into the density matrix in one DMRG run. Here, the maximum number of the Lanczos step for expansion of each $|\omega\rangle$ is taken to be $n_{\rm LV} = 400$. When $g = 0$, there is no excitation in the range of order of J. With g, small weight appears in this range. The absolute magnitude of the weight is 10^{-4} times smaller than the weight at an absorption edge near $\omega = U - V - 4t^2/V$. This ratio is not far from experimental data. There are many peaks in the figure, but these are due to finite-size effects. In the thermodynamic limit, it is expected for the peaks to be continuous. The spectral weight starts from $\omega = \omega_0 = 0.1t$, being consistent with the previous theoretical calculations as well as an experimental observation that the edge of the low-energy absorption starts from $\omega = \omega_0$. We also note that the spectra distribute with a width of πJ. This width is also consistent with the width of spinon dispersion.[57),58)] This is a demonstration of phonon-assisted spin excitations in the presence of EP interaction.

§5. Summary

In order to understand the interplay of strong electron correlation and electron-phonon interaction in 1D Mott insulators, we examine the single-particle excitation spectrum as well as the current-current correlation function in an 1D Hubbard-Holstein model at half-filling. We have employed the dynamical density matrix renormalization group that is powerful for investigating dynamical properties in 1D systems. We have found that the single-particle spectral function is qualitatively explained by a simple superposition scheme of spectra for a spinless carrier dressed with phonons. The superposition is a consequence of robustness of the decoupling of spin and charge against electron-phonon coupling. The current-current correlation function, which is related to the linear optical absorption spectrum, exhibits a peculiar behavior that the effect of the electron-phonon interaction on an exciton is enhanced by increasing the on-site Coulomb repulsion. The electron-phonon coupling also induces low-energy excitations of the order of the antiferromagnetic exchange interaction, but their weight is very small. We have compared the dynamical DMRG data with experimental data of ARPES and optical absorption spectra, and found that the DMRG data with EP interaction are able to qualitatively explain the experimental data, except for dip structures coming from dispersionless phonon assumed in the calculations. Inclusion of dispersive phonons would be a next step to perform more quantitative comparison with the experiments.

As mentioned in §1, understanding the relaxation process is crucial for making up of the basis for the use of 1D Mott insulators as optical devices. Based on the results obtained in this paper, we expect that the EP interaction may also affect on the relaxation process of the photo-excited states in the Mott insulators. A DMRG study of the relaxation process is now in progress.

Acknowledgements

We would like to thank S. Maekawa, A. Ando, and G. Chifune for collaborations on this subject. This work was supported by the Next Generation Supercomputing Project of Nanoscience Program and a Grant-in-Aid for Scientific Research from MEXT. A part of numerical calculations was performed in the supercomputing facilities in Institute for Solid State Physics, University of Tokyo, Yukawa Institute for Theoretical Physics and Academic Center for Computing and Media Studies, Kyoto University, and Institute for Materials Research, Tohoku University. H. M. acknowledges hospitality of YKIS07 organized by the Yukawa International Program for Quark-Hadron Sciences at YITP.

References

1) See, for example, *'Polarons in Bulk Materials and Systems with Reduced Dimensionality', Proceedings of the International School of Physics "Enrico Fermi" Course CLXI*, ed. G. Iadonisi, J. Ranninger and G. De Filippis (IOS Press, 2006).
2) B. Bäuml, G. Wellein and H. Fehske, Phys. Rev. B **58** (1998), 3663.
3) M. Capone, M. Grilli and W. Stephan, Eur. Phys. J. B **11** (1999), 551.
4) E. Cappelluti and S. Ciuchi, Phys. Rev. B **66** (2002), 165102.

5) K. Tsutsui, T. Tohyama and S. Maekawa, J. Low Temp. Phys. **131** (2003), 257.
6) H. Fehske, G. Wellein, G. Hager, A. Weiße and A. R. Bishop, Phys. Rev. B **69** (2004), 165115.
7) W.-Q. Ning, H. Zhao, C.-Q. Wu and H.-Q. Lin, Phys. Rev. Lett. **96** (2006), 156402.
8) H. Matsueda, T. Tohyama and S. Maekawa, Phys. Rev. B **74** (2006), 241103(R).
9) E. Cappelluti, S. Ciuchi and S. Fratini, Phys. Rev. B **76** (2007), 125111.
10) S, Maekawa, T. Tohyama, S. E. Barnes, S. Ishihara, W. Koshibae and G. Khaliullin, *Physics of Transition Metal Oxides* (Splinger-Verlag, Berlin, 2004).
11) W. Stephan and K. Penc, Phys. Rev. B **54** (1996), R17269.
12) F. Gebhard, K. Bott, M. Scheidler, P. Thomas and S. W. Koch, Philos. Mag. **75** (1997), 47.
13) Y. Mizuno, K. Tsutsui, T. Tohyama and S. Maekawa, Phys. Rev. B **62** (2000), R4769.
14) H. Kishida, M. Ono, K. Miura, H. Okamoto, M. Izumi, T. Manako, M. Kawasaki, Y. Taguchi, Y. Tokura, T. Tohyama, K. Tsutsui and S. Maekawa, Phys. Rev. Lett. **87** (2001), 177401.
15) See, for example, P. N. Butcher and D. Cotter, *The Elements of Nonlinear Optics* (Cambridge University Press, Cambridge, 1990).
16) H. Kishida, H. Matsuzaki, H. Okamoto, T. Manabe, M. Yamashita, Y. Taguchi and Y. Tokura, Nature **405** (2000), 929.
17) T. Ogasawara, M. Ashida, N. Motoyama, H. Eisaki, S. Uchida, Y. Tokura, H. Ghosh, A. Shukla, S. Mazumdar and M. Kuwata-Gonokami, Phys. Rev. Lett. **85** (2000), 2204.
18) T. Tohyama and S. Maekawa, J. Luminescence **94-95** (2001), 659.
19) R. Neudert, M. Knupfer, M. S. Golden, J. Fink, W. Stephan, K. Penc, N. Motoyama, H. Eisaki and S. Uchida, Phys. Rev. Lett. **81** (1998), 657.
20) H. Matsueda, N. Bulut, T. Tohyama and S. Maekawa, Phys. Rev. B **72** (2005), 075136.
21) K. Iwano, Phys. Rev. B **74** (2006), 125104.
22) H. Matsueda, A. Ando, T. Tohyama and S. Maekawa, Phys. Rev. B **77** (2008), 193112.
23) A. S. Mishchenko and N. Nagaosa, Phys. Rev. Lett, **93** (2004), 036402.
24) O. Rösch, O. Gunnarsson, X. J. Zhou, T. Yoshida, T. Sasagawa, A. Fujimori, Z. Hussain, Z.-X. Shen and S. Uchida, Phys. Rev. Lett. **95** (2005), 227002.
25) J. Bonča, S. Maekawa, T. Tohyama and P. Prelovšek, Phys. Rev. B **77** (2008), 054519.
26) A. S. Mishchenko, N. Nagaosa, Z.-X. Shen, G. De Filippis, V. Cataudella, T. P. Devereaux, C. Bernhard, K. W. Kim and J. Zaanen, Phys. Rev. Lett. **100** (2008), 166401.
27) S. R. White, Phys. Rev. Lett. **69** (1992), 2863; Phys. Rev. B **48** (1993), 10345.
28) K. A. Hallberg, Phys. Rev. B **52** (1995), R9827.
29) T. D. Kühner and S. R. White, Phys. Rev. B **60** (1999), 335.
30) E. Jeckelmann, Phys. Rev. B **66** (2002), 045114.
31) H. Benthien, F. Gebhard and E. Jeckelmann, Phys. Rev. Lett **92** (2004), 256401.
32) N. Shibata, J. of Phys. A **36** (2003), R381.
33) K. A. Hallberg, Adv. Phys. **55** (2006), 477.
34) G. Khalliulin and P. Horsch, Physica C **282-287** (1997), 1751.
P. Horsch and G. Khaliullin, cond-mat/0501239.
P. Horsch, G. Khaliullin and V. Oudovenko, Physica C **341-348** (2000), 117.
35) O. Rösch and O. Gunnarsson, Phys. Rev. Lett. **92** (2004), 146403; Phys. Rev. B **70** (2004), 224518.
36) E. Jeckelmann and S. R. White, Phys. Rev. B **57** (1998), 6376.
37) B. J. Kim, H. Koh, E. Rotenberg, S.-J. Oh, H. Eisaki, N. Motoyama, S. Uchida, T. Tohyama, S. Maekawa, Z.-X. Shen and C. Kim, Nature Phys. **2** (2006), 397.
38) E. H. Lieb and F. Y. Wu, Phys. Rev. Lett. **20** (1968), 1445.
39) M. Ogata and H. Shiba, Phys. Rev. B **41** (1990), 2326.
40) A. Parola and S. Sorella, Phys. Rev. B **45** (1992), 13156.
S. Sorella and A. Parola, J. of Phys.: Cond. Mat. **4** (1992), 3589.
41) H. Suzuura and N. Nagaosa, Phys. Rev. B **56** (1997), 3548.
42) M. Hohenadler, M. Aichhorn and W. von der Linden, Phys. Rev. B **68** (2003), 184304.
43) S. Sykora, A. Hubsch, K. W. Becker, G. Wellein and H. Fehske, Phys. Rev. B **71** (2005), 045112.
44) Hui Zhao, C. Q. Wu and H. Q. Lin, Phys. Rev. B **71** (2005), 115201.
45) C. Zhang, E. Jeckelmann and S. R. White, Phys. Rev. B **60** (1999), 14092.

46) V. V. Kabanov and O. Yu. Mashtakov, Phys. Rev. B **47** (1993), 6060.
47) J. Bonča, S. A. Trugman and I. Batistić, Phys. Rev. B **60** (1999), 1633.
48) G. Wellein and H. Fehske, Phys. Rev. B **56** (1997), 4513.
49) P. Prelovšek, R. Zeyher and P. Horsch, Phys. Rev. Lett. **96** (2006), 086402.
50) A. Ramšak, P. Horsch and P. Fulde, Phys. Rev. B **46** (1992), 14305.
51) G. Wellein, H. Röder and H. Fehske, Phys. Rev. B **53** (1996), 9666.
52) H. Matsueda, T. Tohyama and S. Maekawa, Phys. Rev. B **70** (2004), 033102; Phys. Rev. B **71** (2005), 153106.
53) Gerald D. Mahan, *Many-Particle Physics, third edition* (Kluwer Academic / Plenum Publishers, New York, 2000).
54) M. Ono, K. Miura, A. Maeda, H. Matsuzaki, H. Kishida, Y. Taguchi, Y. Tokura, M. Yamashita and H. Okamoto, Phys. Rev. B **70** (2004), 085101.
55) M. Yoshida, S. Tajima, N. Koshizuka, S. Tanaka, S. Uchida and S. Ishibashi, Phys. Rev. B **44** (1991), 11997.
56) J. Lorenzana and G. A. Sawatzky, Phys. Rev. Lett. **74** (1995), 1867; Phys. Rev. B **52** (1995), 9576.
57) H. Suzuura, H. Yasuhara, A. Furusaki, N. Nagaosa and Y. Tokura, Phys. Rev. Lett. **76** (1996), 2579.
58) J. Lorenzana and R. Eder, Phys. Rev. B **55** (1997), R3358.